IEEE Photonics Journal
An IEEE Photonics Society Publication

Open Access

Optimization of Illumination Performance of Trichromatic White Light-Emitting Diode and Characterization of Its Modulation Bandwidth for Communication Applications

Volume 10, Number 5, September 2018

Hua Xiao
Xiangtian Xiao
Kai Wang
Rui Wang
Bin Xie
Kin Seng Chiang, *Member, IEEE*

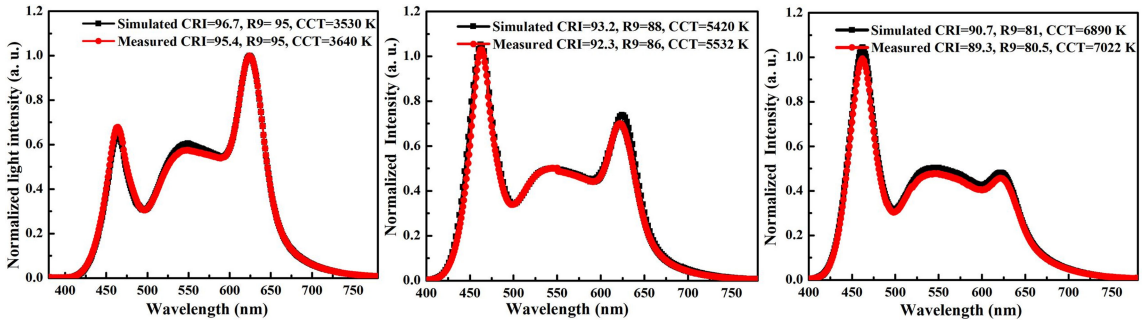

DOI: 10.1109/JPHOT.2018.2872565

Optimization of Illumination Performance of Trichromatic White Light-Emitting Diode and Characterization of Its Modulation Bandwidth for Communication Applications

Hua Xiao,[1] **Xiangtian Xiao**,[2] **Kai Wang**,[2] **Rui Wang**,[2] **Bin Xie**,[3] **and Kin Seng Chiang**,[1] ***Member, IEEE***

[1]Department of Electronic Engineering, City University of Hong Kong, Hong Kong
[2]Department of Electrical and Electronic Engineering, Southern University of Science and Technology, Shenzhen 518055, China
[3]State Key Laboratory of Coal Combustion and Thermal Packaging Laboratory, School of Energy and Power Engineering, Huazhong University of Science and Technology, Wuhan 430074, China

DOI:10.1109/JPHOT.2018.2872565

Manuscript received August 20, 2018; revised September 17, 2018; accepted September 24, 2018. Date of publication October 1, 2018; date of current version October 9, 2018. This work was supported in part by the National Natural Science Foundation of China under Grant 51402148, in part by the Guangdong High Tech Project under Grant 2014TQ01C494, in part by the Distinguished Young Scholar of Natural Science Foundation of Guangdong (2017B030306010), and in part by the Shenzhen Innovation Project under Grant JCYJ20160301113537474. *(Hua Xiao and Xiangtian Xiao contributed equally to this work.)*
Corresponding authors: Kai Wang and Rui Wang (e-mail: wangk@sustc.edu.cn; wangr@sustc.edu.cn).

Abstract: We study a trichromatic white light-emitting diode (WLED) system that consists of a blue LED covered with layers of red emissive CdSe/ZnS quantum dots (QDs) and yellow emissive YAG:Ce^{3+} phosphors. With the knowledge of the individual emission spectra of the blue LED, the QDs, and the phosphors, we develop a method of determining the right amounts of QDs and phosphors to optimize the illumination performance of the WLED. The predicted performances of the WLEDs obtained from our method agree well with experimental results. With this method, we are able to produce white light with, for example, a high color-rendering index of 95.4 and an R9 value of 95.0 at a correlated color temperature (CCT) of 3640 K. We also analyze the modulation characteristics of this WLED system for visible light communication (VLC). By combining the frequency responses of the blue LED, the QDs, and the phosphors, we are able to accurately predict the overall frequency responses and the bandwidths of the WLEDs that have various CCTs and, thus, optimize the bandwidth of the WLED. Our approach of optimizing the performance of a WLED, as verified by our measurement data, is simple and general and can facilitate the selection of suitable light-conversion materials for combined illumination and VLC applications.

Index Terms: Light-emitting diodes, optical materials, quantum-dot devices, optical communication.

1. Introduction

Light-emitting diodes (LEDs) are expected to become the next generation of solid-state light sources for illumination and communication applications for their numerous advantages, such as

eco-friendliness, long life span, high reliability, high efficiency, modulation ability, compact size, short carrier lifetime, low junction capacity, and high endurance of high-frequency injection currents [1]–[3]. Currently, the most widely used approach to generating white LED (WLED) light with high color-rendering index (CRI) is to convert blue LED light into yellow light with yellow-emissive cerium-doped yttrium aluminum garment ($Y_3Al_5O_{12}$: Ce^{3+}, YAG) phosphors together with red-emissive phosphors [4], [5]. However, commercial red phosphors suffer from low efficiency in illumination [6] and slow response in communication [7]. To achieve high performance in both illumination and modulation for visible light communication (VLC), quantum dots (QDs) have been proposed to replace red phosphors for their distinguished properties, such as tunable emission wavelength, high quantum efficiency, narrow spectral width at deep-red wavelengths, and short fluorescent lifetime [8], [9]. QDs can compensate for the yellow-dominated spectrum of conventional WLED light to produce a high value of R9 [10]–[12], which is a colorimetric index for the evaluation of saturated red color and is normally used in biomedical and painting identification. By using purely empirical approaches, however, it has been difficult to realize QD-based WLEDs with both high CRI ($>$90) and R9 ($>$90) values at given correlated color temperature (CCT) values between 3000 K and 7000 K [1], [9], [13]–[15]. Up to now, no general method is available for generating WLED light with both optimized CRI and R9 values.

In this paper, we describe a general method to simultaneously obtain high CRI and R9 values at a given CCT value for a trichromatic WLED, which consists of three elements: a blue LED, CdSe/ZnS QDs, and YAG phosphors. In comparison with blue QDs [16], a blue LED can provide more stable and controllable output. Alloyed CdSe/ZnS QDs [17] can offer much more stable chemical characteristics than other QDs, such as perovskite QDs [18]. CdSe/ZnS QDs have in fact been adapted and integrated in other optoelectronic devices, such as solar cells [19], electroluminescence-based LEDs [20], and lasers [21]. YAG phosphors emit a broad spectrum of yellow light and can nicely fill the spectral gap between the blue LED and the CdSe/ZnS QDs. All these elements are commercially available. From the individual emission spectra of these elements and the target white-light spectrum, we are able to determine the right proportions of the QDs and the phosphors for a desired illumination performance. Our preliminary study has confirmed the feasibility of the method [22]. We also investigate the modulation characteristics of the QD-based WLED for VLC applications. By measuring the frequency responses of the three elements, we can synthesize the overall frequency response of the WLED for a given illumination performance. While light sources, such as laser diodes [23], micro LEDs [24], [25], and RGB LEDs [26], [27], have been applied to high-speed VLC, they are expensive and not designed for large-area illumination. A fluorescent WLED source can be a more cost-effective option, which can also offer high color tunability [28], [29]. So far, the studies on fluorescent WLEDs for VLC applications have been focused mainly on their communication performance; there has been no report on optimizing their illumination performance. Our present study provides a general approach of simultaneously optimizing the illumination and communication performances of QD-based fluorescent trichromatic WLEDs.

2. Optimization of Illumination Performance

We consider a WLED system that consists of a blue LED chip, CdSe/ZnS QDs, and YAG phosphors. Our objective is to determine the proportions of the QDs and the phosphors with an algorithm, so that the WLED light generated have optimized CRI and R9 values for a given CCT value.

2.1 Setup of the WLED

Figure 1(a) shows a lead frame packaged blue LED chip (Hualian Electronics Co. Ltd) bonded on an aluminum substrate with negative and positive anodes. The dimensions of the chip are $200 \times 300\,\mu m^2$. Layers of silicone mixed CdSe/ZnS QDs (Poly OptoElectronics Co., Ltd) and YAG phosphors (Youyan Rare Earth Co., Ltd) with an individual thickness of 2 mm and a diameter of 11 mm are placed on the LED-substrate module. To prevent reabsorption of the converted light between phosphors and QDs, the blue light emitted by the LED chip first passes through the QD

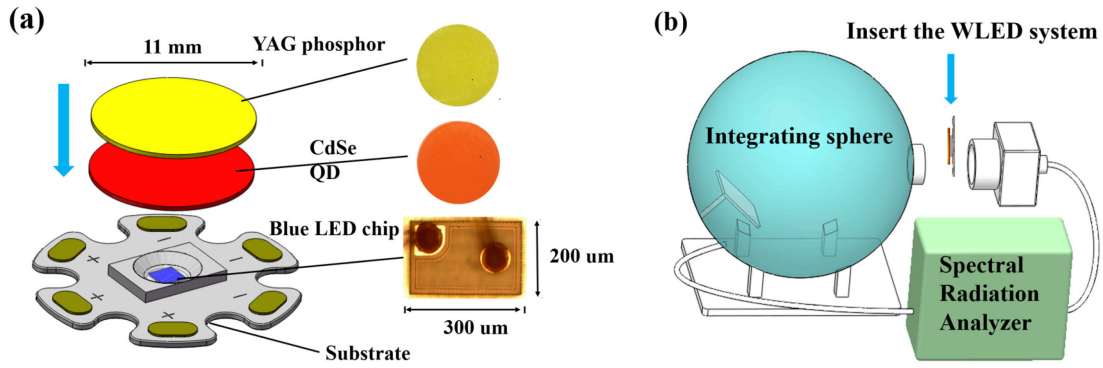

Fig. 1. (a) The WLED system used in our study is a blue LED chip covered with CdSe/ZnS QD and YAG phosphor layers. (b) The output light from the WLED system is measured with an integrating sphere connected to a spectral radiation analyzer.

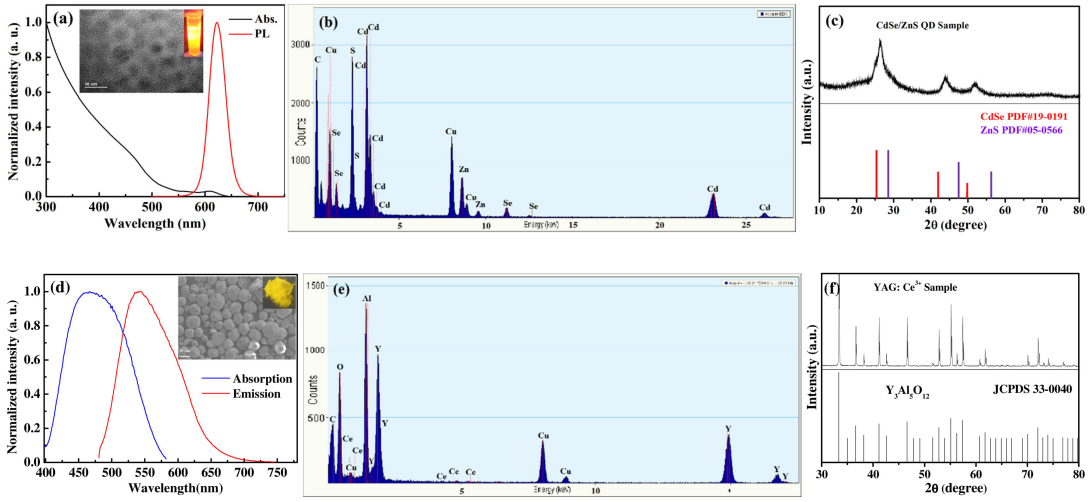

Fig. 2. (a) Absorption and emission spectra, (b) EDX analysis, and (c) XRD analysis of the CdSe/ZnS QDs; (d) absorption and emission spectra, (e) EDX analysis, and (f) XRD analysis of YAG:Ce phosphors. The Insets in (a) and (d) are a HRTEM image of the CdSe/ZnS QDs and an SEM image of the YAG phosphors, respectively.

layer and then the phosphor layer. Figure 1(b) shows the measurement setup, where the output light from the WLED system is collected by a 500 mm-diameter integrating sphere (Everfine), which is connected to a spectral radiation analyzer (Spectro-320) for the measurement of the spectrum, the optical power, and the CCT, CRI, and R9 values.

Figures 2(a), (b), and (c) show the measured absorption and emission spectra, the energy dispersive X-ray (EDX) analysis, and the X-Ray diffraction (XRD) analysis (Bruker Advance D8 Ew Germany) of the CdSe/ZnS QDs, respectively. The inset in Fig. 2(a) is a high-resolution transmission electron microscopy (HRTEM) (FEI Tecnai G2 F30) image of the QDs, which shows that the average diameter of the QDs is ~7.0 nm. The emission spectrum of the QDs peaks at 625 nm with a narrow full-width-at-half-maximum (FWHM) of 36 nm. Figure 2(b) confirms the chemical components in the CdSe/ZnS QDs and Fig. 2(c) confirms the purities of CdSe and ZnS in the alloy. Figures 2(d), (e), and (f) show the measured absorption and emission spectra, the EDX analysis, and the XRD analysis of the YAG phosphors, respectively. The inset in Fig. 2(d) is a scanning electron microscopy (SEM) image of phosphors, which shows that the average diameter of the phosphors is ~8.2 μm. The absorption and emission spectra of the phosphors peak at 460 nm and 550 nm, respectively. The EDX and XRD results confirm the expected compositions in the YAG phosphors.

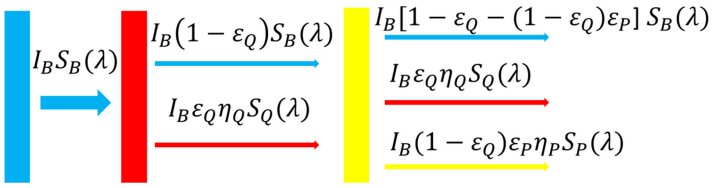

Fig. 3. Illustration of the light beams passing through various layers of the WLED system.

2.2 Generation of the WLED Spectrum

Figure 3 illustrates the light beams passing through various layers of the WLED system. The normalized spectrum of the output light from the WLED system $S_W(\lambda)$ (with λ being the free-space wavelength) can be expressed as

$$I_W S_W(\lambda) = I_B \left[M_B S_B(\lambda) + M_Q S_Q(\lambda) + M_P S_P(\lambda)\right], \tag{1}$$

with

$$M_B = (1-\varepsilon_Q) - (1-\varepsilon_Q)\varepsilon_P, \tag{2}$$

$$M_Q = \varepsilon_Q \eta_Q, \tag{3}$$

$$M_P = (1-\varepsilon_Q)\varepsilon_P \eta_p, \tag{4}$$

where $S_B(\lambda)$, $S_Q(\lambda)$, and $S_P(\lambda)$ are the normalized emission spectra of the blue LED, the QDs, and the phosphors, respectively; I_W and I_B are the light intensities of the WLED output and the blue LED output, respectively; ε_Q and ε_P are the fractions of the blue LED light converted by the QDs and the phosphors, respectively; and η_Q and η_P are the quantum efficiencies of the QDs and the phosphors, respectively. The parameters M_B, M_Q, and M_P are the optical conversion efficiencies for the blue LED, the QDs, and the phosphors, respectively, which are defined as

$$M = \frac{P_e(\lambda)}{P_a(\lambda)} = \frac{\int_{380}^{780} P_e(\lambda)d\lambda}{\int_{380}^{780} P_a(\lambda)d\lambda}, \tag{5}$$

where $P_a(\lambda)$ and $P_e(\lambda)$ are the powers of the absorbed light and the emitted light for the element of concern, namely, the blue LED, the QDs, or the phosphors.

Figure 4(a) shows the measured emission spectra of the blue LED, the QDs, and the phosphors, i.e., $S_B(\lambda)$, $S_Q(\lambda)$, and $S_P(\lambda)$, where $S_Q(\lambda)$, and $S_P(\lambda)$ are the same as the emission spectra shown in Fig. 2(a) and (b). The spectrum of the blue LED was measured at an injection current of 50 mA, which delivered an optical power of 169 mW. Our task is to search for the values of M_B, M_Q, and M_P with the knowledge of $S_B(\lambda)$, $S_Q(\lambda)$, and $S_P(\lambda)$, so that the WLED spectrum generated from Eq. (1) gives the largest CRI and R9 values at a given CCT value. To achieve this, we develop a simulated annealing algorithm [30] and implement it with Matlab. The algorithm searches for the WLED spectrum (i.e., the values of M_B, M_Q, and M_P) that produces a CCT value close to the target value and, at the same time, offers the largest possible CRI and R9 values. The optimization goal of the algorithm is expressed as

$$f = \Delta \times (a_1 g_1 + a_2 g_2 + a_3 g_3), \tag{6}$$

With

$$g_1 = 0, \text{ if } \frac{|CCT_{est} - CCT_{tar}|}{CCT_{tar}} < \varepsilon$$

$$g_1 = \left(\frac{|CCT_{est} - CCT_{tar}|}{CCT_{tar}} - \varepsilon\right) \Big/ \varepsilon, \text{ if } \frac{|CCT_{est} - CCT_{tar}|}{CCT_{tar}} > \varepsilon \tag{7}$$

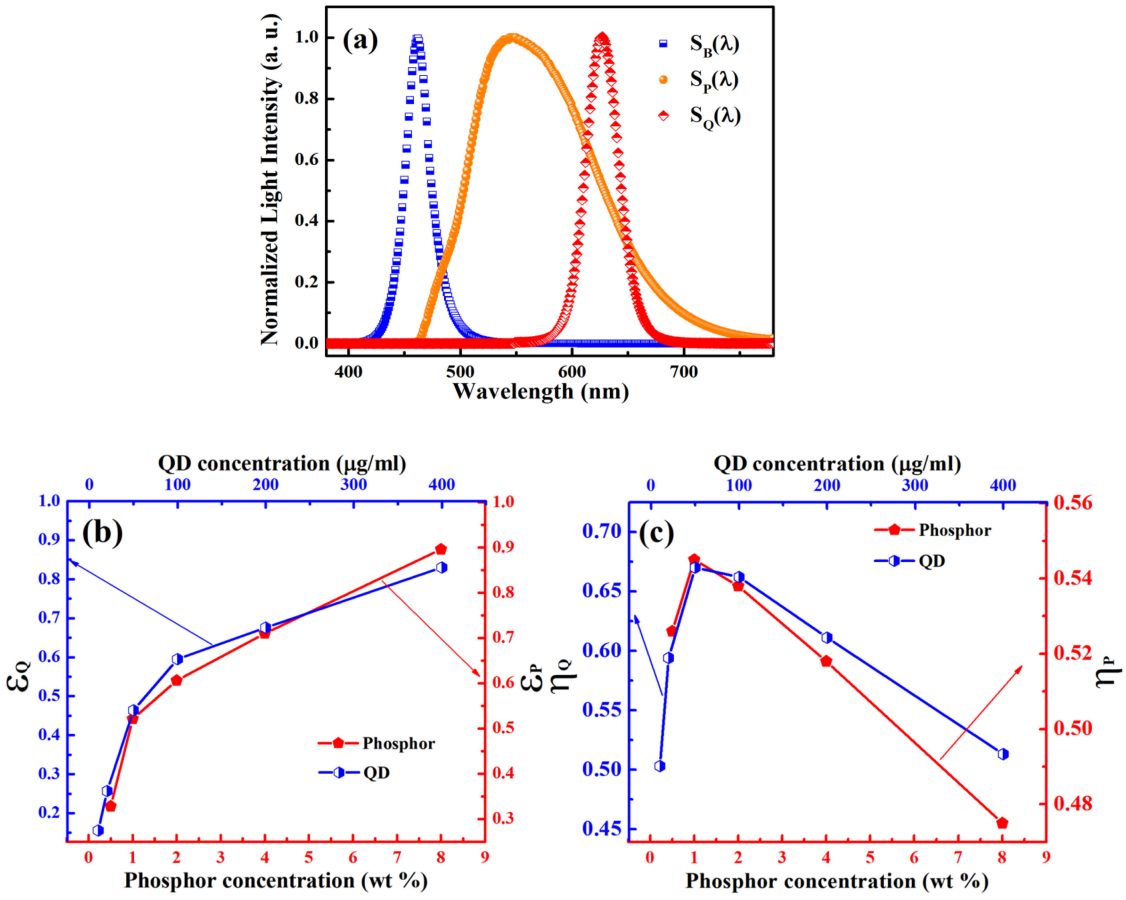

Fig. 4. (a) Measured spectra of the blue LED, the QDs, and the phosphors for the WLED. Variations of (b) ε_Q and ε_P and (c) η_Q and η_P with the QD and phosphor concentrations.

$$g_2 = 0, \text{f}\ \frac{|CRI_{\text{est}} - CRI_{tar}|}{CRI_{tar}} < \varepsilon$$
$$g_2 = \left(\frac{|CRI_{est} - CRI_{tar}|}{CRI_{tar}} - \varepsilon\right) \Big/ \varepsilon, \text{if}\ \frac{|CRI_{est} - CRI_{tar}|}{CRI_{tar}} > \varepsilon \tag{8}$$

and

$$g_3 = 0, \text{if}\ \frac{|R9_{\text{est}} - R9_{tar}|}{R9_{tar}} < \varepsilon$$
$$g_3 = \left(\frac{|R9_{est} - R9_{tar}|}{R9_{tar}} - \varepsilon\right) \Big/ \varepsilon, \text{if}\ \frac{|R9_{est} - R9_{tar}|}{R9_{tar}} > \varepsilon \tag{9}$$

where CCT_{est} , CRI_{est} , and $R9_{est}$ are the estimated values of CCT, CRI, and R9, which are calculated from $S_W(\lambda)$, CCT_{tar}, CRI_{tar}, and $R9_{tar}$ are the corresponding target values set by the user, and ε is the error between the estimated value and the target value. a_1, a_2, and a_3 are the weighting coefficients of g_1, g_2, and g_3, respectively, which are set to control the relative importance of CCT, CRI, and R9 in the optimization process. Δ, an expansion factor usually larger than 2000, is set to accelerate the optimization process. In our calculation, we set $a_1 = a_2 = a_3 = 0.333$, $\Delta = 5000$, and $\varepsilon = 0.02$. The optimization objective is to minimize the value of f. The details for the evaluation of CCT, CRI, and R9 of a spectrum can be found in [31] and [32].

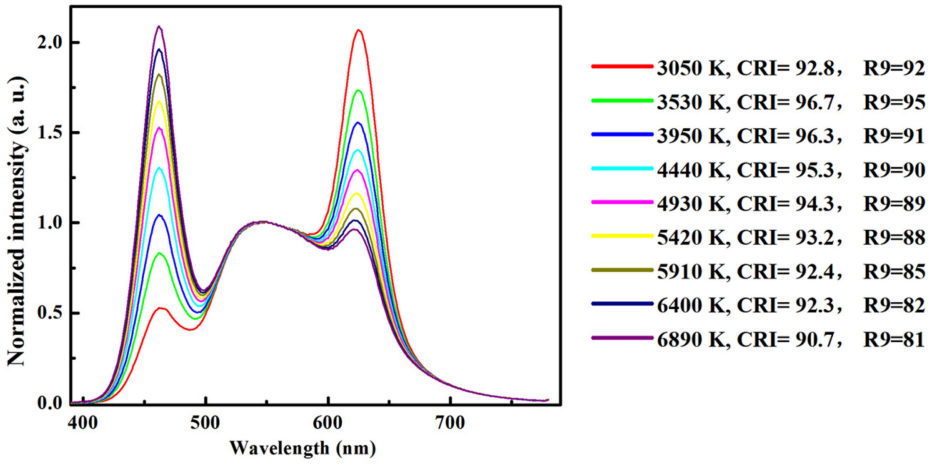

Fig. 5. Spectral power distribution for CRI optimized WLED with CCT value ranges from 3000 to 7000 K.

TABLE 1
Parameters for the WLED System

CCT (K)	3050	3530	3950	4440	4930	5420	5910	6400	6890
M_B	0.080	0.136	0.147	0.202	0.237	0.273	0.310	0.328	0.367
M_Q	0.269	0.238	0.220	0.211	0.198	0.189	0.180	0.172	0.166
M_P	0.128	0.138	0.144	0.150	0.153	0.166	0.171	0.171	0.172

According to Eqs. (1)–(4), the values of M_B, M_Q, and M_P are related to the values of ε_Q, ε_P, η_Q, and η_P, which depend on the concentrations of the QDs and the phosphors. To determine the dependences of ε_Q and η_Q on the QD concentration, we measure the transmitted spectrum from the QD layer only (prepared at a known QD concentration) and calculate ε_Q with the output spectrum and the blue-light spectrum and η_Q with the procedure described in Ref. 4. We repeat the measurements for QD layers prepared with different known QD concentrations. The results are shown in Fig. 4(b). We determine the dependences of ε_P and η_P on the phosphor concentration in the same way and the results are shown in Fig. 4(c). These results allow us to determine the QD and phosphor concentrations to achieve the desired values of M_B, M_Q, and M_P.

2.3 Numerical Results and Experimental Verification

Figure 5 shows a number of WLED spectra optimized at CCT values ranging from 3000 to 7000 K, which belong to the normal range of white-light CCT values. The CRI and R9 values for each spectrum are the largest we can achieve at the specified CCT value. As shown in Fig. 5, the CRI and R9 values increase first and then decrease with an increase in the CCT value with peak values at CCT $=$ 3530 K. The CRI values in all the generated spectra are larger than 90, which indicates excellent illumination performance in all these cases. The corresponding values of M_B, M_Q, and M_P for the spectra shown in Fig. 5 are listed in Table 1.

We should note that our results are insensitive to the injection current applied to the blue LED. We measured the variation of the emission spectrum of the blue LED with the injection current and found that the peak wavelength of the spectrum shifted by only $\sim$0.5 nm (from 461.8 to 462.3 nm)

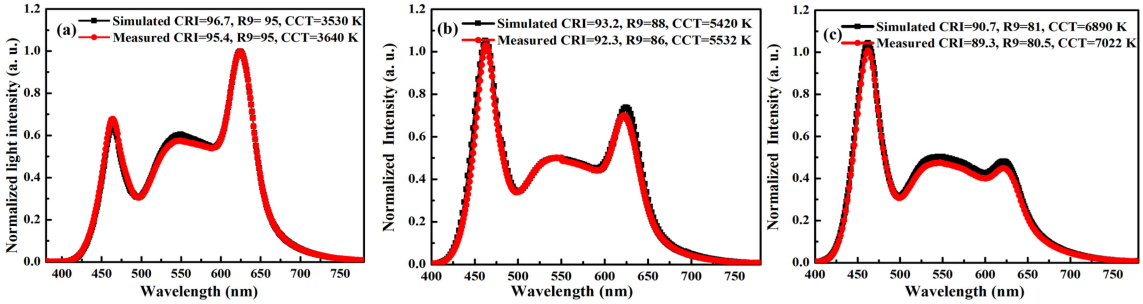

Fig. 6. Comparison of calculated and measured spectra of WLEDs with three different target CCT values. (a) 3530 K. (b) 5420 K. (c) 6890 K.

with the injection current varying from 20 to 80 mA. The corresponding change in the absorption of the QDs is only ~0.1%, which can hardly affect the results.

For experimental verification, we consider three WLED spectra with CCT = 3530, 5420, and 6890 K. As shown in Table 1, the values of M_B, M_Q, and M_P required are 0.136, 0.238, and 0.138, respectively, for CCT = 3530 K; 0.273, 0.189, and 0.166, respectively, for CCT = 5420 K; and 0.367, 0.166, and 0.172, respectively, for CCT = 6890 K. From Eqs. (2)–(4), for CCT = 3530 K, the corresponding values of ε_Q, ε_P, η_Q, and η_P are 0.42, 0.63, 0.53, and 0.62, respectively, which can be achieved with a QD concentration of 40 μg/ml and a phosphor concentration of 3 wt%. For CCT = 5420 K, the values of ε_Q, ε_P, η_Q, and η_P are 0.28, 0.58, 0.62, and 0.51, respectively, which can be achieved with a QD concentration of 30 μg/ml and a phosphor concentration of 3.5 wt%. For CCT = 6890 K, the values of ε_Q, ε_P, η_Q, and η_P are 0.3, 0.45, 0.6, and 0.55, respectively, which can be achieved with a QD concentration of 32 μg/ml and a phosphor concentration of 1 wt%. We prepared three WLEDs with the required concentrations of QDs and phosphors and measured their CCT, CRI, and R9 values together with the output spectra $S_W(\lambda)$. The results for the three WLEDs are shown in Figs. 6(a), (b), and (c), respectively. As shown in Fig. 6, the measured output spectra of the WLEDs agree well with those calculated by our optimization method. For example, for a target CCT value of 3530 K, the actual CCT value obtained is 3640 K and the CRI and R9 values are 95.4 and 95.0, respectively, which are also close to the calculated values. The results in Fig. 6 confirm that our method is accurate for the determination of the QD and the phosphor concentration required for obtaining the desired illumination performance with the WLED over a wide range of color temperatures. The CRI values we achieve are higher than those obtained using yellow and red phosphors [4], QD-PMMA [9], carbon dots [14], and phosphors in glass [33].

3. Characterization of Modulation Performance

According to recent surveys, commercial WLED systems can offer bandwidths of approximately 1 MHz [34], [35]. Thanks to the short fluorescence time [36] and the fast response [7] of QDs, QD-based WLEDs should perform better than traditional WLEDs for VLC applications. In this section, we provide an analysis of the frequency response of our WLED. We show explicitly how the frequency responses of the blue LED chip, the QDs, and the phosphors contribute to the frequency response of the WLED. With our analysis, it becomes possible to predict the frequency response of the WLED in optimizing the illumination performance. As such, we can establish a relationship between the illumination performance and the modulation performance of the WLED.

3.1 Calculation of the Frequency Response of the WLED

The frequency response of the WLED, $R(f)$, can be expressed as

$$R(f) = M_B R_B(f) + M_Q R_Q(f) + M_P R_P(f) \tag{10}$$

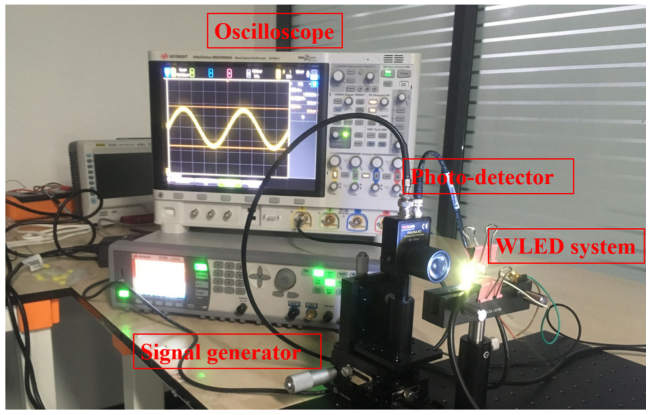

Fig. 7. Experimental setup for the measurement of the frequency response of the WLED.

where $R_B(f)$, $R_Q(f)$, and $R_P(f)$ are the normalized frequency responses of the blue LED, the QDs, and the phosphors, respectively. The response of the blue LED, $R_B(f)$, depends on the injection current, while the responses of the QDs and the phosphors, $R_Q(f)$ and $R_P(f)$ are the properties of the materials. M_B, M_Q, and M_P are the conversion efficiencies that governs the illumination performance, which can be found from the method described in Section 2. With Eq. (10), we can predict the frequency responses of WLEDs formed with any combinations of QD and phosphor concentrations from the frequency responses of the individual components $R_B(f)$, $R_Q(f)$, and $R_P(f)$, which only need to be measured once.

3.2 Comparison With Measurement Results

Figure 7 shows the experimental setup for the measurement of the frequency responses of the WLED and its elements. The blue LED was properly biased and driven with a signal generator (RIGOL DG5072). The output light from the WLED was monitored with a photodetector (THORLABS PDA10A, 150 MHz) and an oscilloscope (KEYSIGHT, InfiniiVison MSOX6004A). The frequency response of the blue LED alone, $R_B(f)$, was measured with the QD and phosphor layers removed from the WLED. To measure the frequency responses of the QD and phosphor layers, a blue filter was used to eliminate any blue light from the blue LED. Figure 8(a) shows the measured frequency responses $R_B(f)$, $R_Q(f)$, and $R_P(f)$. Their 3-dB bandwidths are 8.1 MHz, 3.4 MHz, and 1.8 MHz, respectively. The bandwidth of QDs is significantly wider than that of phosphors. As an example, for an WLED with a CCT value of 3300 K, the values of M_B, M_Q, and M_P are 0.118, 0.247, and 0.132, respectively. We calculate the frequency response of this WLED from Eq. (10) and compare it with the measured frequency response. Note that the 3-dB optical bandwidth of the WLED is equivalent to the width of the electrical response where the amplitude drops to 0.707 of its peak value. As shown in Fig. 8(b), the agreement between the calculated response and the measured response is good, which confirms that Eq. (10) is an accurate expression for predicting the frequency response of the WLED. The 3-dB bandwidth of the WLED is $\sim$3 MHz, which is mainly limited by the bandwidth of the phosphors. Figure 8(c) compares the calculated 3-dB bandwidths and the measured 3-dB-bandwidths for WLEDs optimized at different CCT values. The agreement is in general good. The smallest bandwidth achieved is 3.11 MHz (at CCT $\sim$ 4000 K), which is wider than those of commercial WLEDs. The bandwidth of the WLED could be further increased by adding blue filtering [37] or using orthogonal-frequency-division multiplexing (OFDM) [38], analog pre-equalizer [39], or analog post-equalizer [40]. Our illumination-optimized WLEDs can be readily applied to indoor illumination and communication [41], [42].

Figure 8(c) shows the dependence of the bandwidth of the illumination-optimized WLED on the CCT value. As shown in Fig. 8(c), the bandwidths calculated from Eq. (10) (the curve labelled

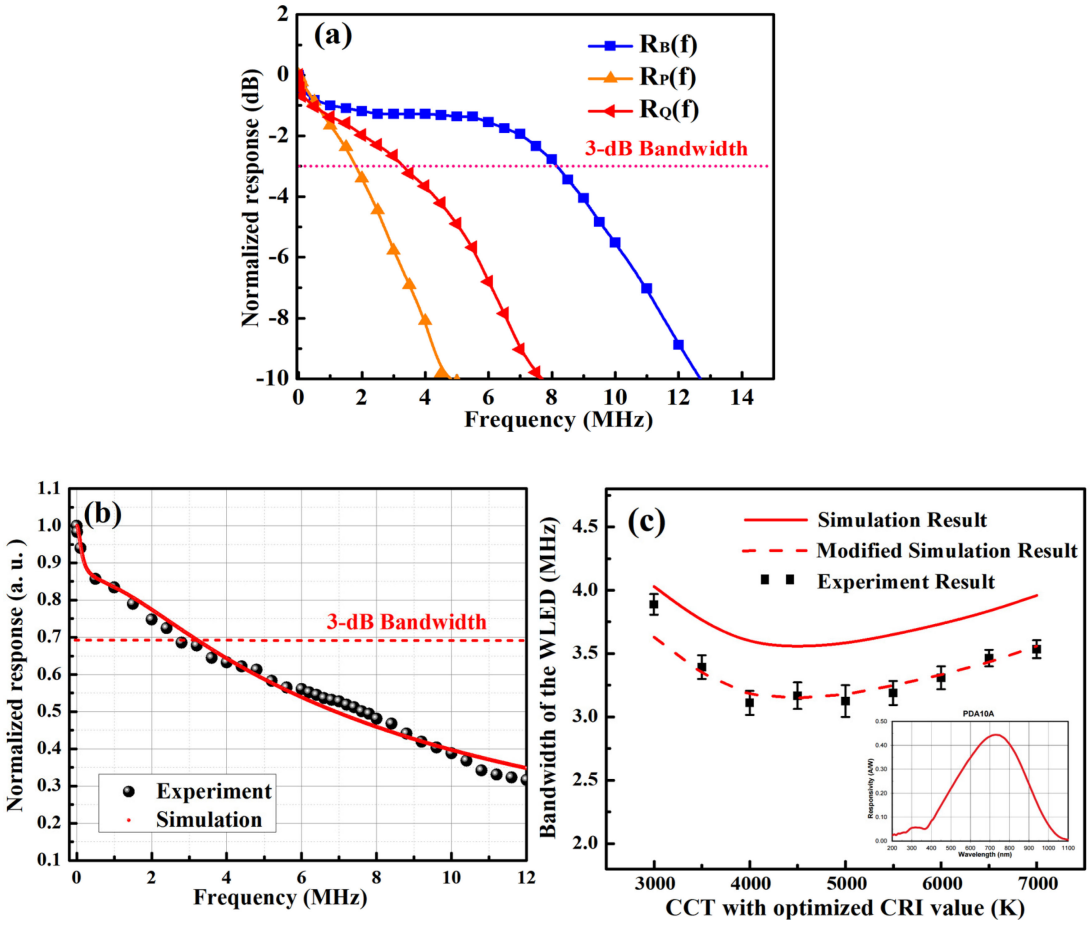

Fig. 8. (a) Normalized frequency responses of $R_B(f)$, $R_Q(f)$, and $R_P(f)$. (b) Comparison of calculated and measured frequency responses of an illumination-optimized WLED that has a CCT of 3300 K. (c) Comparison of calculated and measured bandwidths for illumination-optimized WLEDs that have different CCT values, where the inset shows the responsivity of the photodetector (PDA10A) [34].

as “Simulation Result”) are larger than the measured bandwidths (the data points labelled as “Experimental Result”). The discrepancies can be explained by the wavelength dependence of the responsivity of the silicon photo-detector [43] used in our experiments. As shown in the inset of Fig. 8(c), the responsivity decreases with the wavelength in the visible regime. As a result, the contribution from the blue LED (which has the widest bandwidth) to the measured frequency response of the WLED is deemphasized, which thus leads to a smaller measured bandwidth. To take into account the wavelength dependence of the responsivity of the photo-detector in the calculation of the frequency response of the WLED, we multiply the values 0.16, 0.27, and 0.37 to the three terms in Eq. (10) that contain $R_B(f)$, $R_P(f)$, and $R_Q(f)$, respectively. These values correspond to the peak wavelengths of $R_B(f)$ (455 nm), $R_P(f)$ (550 nm), and $R_Q(f)$ (625 nm), respectively. With this modification, the calculated bandwidths, shown by the curve labelled as “Modified Simulation Result” in Fig. 8(c), agree well with the measured bandwidths. As shown in Fig. 8(c), when the CCT value increases, the bandwidth tends to decrease first and then increase slowly again, which can be explained from the results in Table 1. At a small CCT value, the red component generated from the QDs well dominates over the yellow component generated from the phosphors, so the bandwidth is larger. As the CCT values increases, the yellow component becomes more significant and the bandwidth becomes smaller. As the CCT value increases further, however, the blue component generated from the blue LED chip becomes significant enough to increase the bandwidth again.

The results shown in Fig. 8 were obtained at an injection current of 50 mA to the blue LED. Although the frequency response of the blue LED is sensitive to the injection current, the bandwidth of the WLED, which is limited by the phosphors and the QDs, should be relatively insensitive to the injection current (which is particularly the case at a low CCT where the M_B value is small). We may obtain a more accurate estimate of the bandwidth of the WLED at any other injection current by using the frequency response of the blue LED measured at the injection current of concern.

4. Conclusion

We demonstrate a method of optimizing the illumination performance of a tri-chromatic WLED that consists of a blue LED, CdSe/ZnS QDs, and YAG phosphors. This method allows us to easily determine the proper QD and phosphor concentrations for the achievement of optimal illumination performance, i.e., maximum CRI and R9 values, at a specified CCT. In addition, we are able to accurately predict the frequency response of the illumination-optimized WLED from the frequency responses of the blue LED, the QDs, and the phosphors. The calculated frequency response agrees well with the measurement results. As such, we successfully establish a relationship between the illumination performance and the communication performance of the WLED, which can facilitate the implementation of the WLED for both illumination and VLC. While we demonstrate our idea with a specific WLED system, our approach of optimizing the illumination performance together with the process of characterizing the frequency response can be applied to WLEDs based on other light-conversion materials. Without involving massive empirical experimental work, our method, which is based on numerical calculation with preset measurement data, can greatly accelerate the process of finding the desired recipes of WLEDs produced for various illumination and communication applications.

Acknowledgement

The authors would like to thank H. Yang, W. Zhang, and the Analysis and Testing Center of South University of Science and Technology for their technical assistance.

References

[1] C. Sun *et al.*, "High color rendering index white light emitting diodes fabricated from a combination of carbon dots and zinc copper indium sulfide quantum dots," *Appl. Phys. Lett.*, vol. 104, no. 26, 2014, Art. no. 261106.
[2] G. J. Jeong, J. H. Lee, S. H. Han, W. Y. Jin, J. W. Kang, and S. N. Lee, "Silver nanowires for transparent conductive electrode to GaN-based light-emitting diodes," *Appl. Phys. Lett.*, vol. 106, no. 3, 2015, Art. no. 031118.
[3] Y. K. Lee, Y. H. Kim, J. Heo, W. B. Im, and W. J. Chung, "Control of chromaticity by phosphor in glasses with low temperature sintered silicate glasses for LED applications," *Opt. Lett.*, vol. 39, no. 14, pp. 4084–4087, 2014.
[4] H. Xiao, T. M. Shih, Z. Q. Guo, Y. Lin, Y. J. Lu, and Z. Chen, "3-D microlens phosphor with curvatures manufactured by imprinting for chip-on-board light-emitting diodes," *IEEE Trans. Electron Device*, vol. 63, no. 3, pp. 1128–1133, Mar. 2016.
[5] M. J. Lee, Y. H. Song, Y. L. Song, G. S. Han, H. S. Jung, and D. H. Yoon, "Enhanced luminous efficiency of deep red emitting K2SiF6: Mn4+ phosphor dependent on KF ratio for warm-white LED," *Mater. Lett.*, vol. 141, no. 1, pp. 27–30, 2015.
[6] M. Yamada *et al.*, "Red-enhanced white-light-emitting diode using a new red phosphor," *Jpn. J. Appl. Phys.*, vol. 42, no. 1A, pp. L20–L23, 2003.
[7] X. Xiao *et al.*, "Improving the modulation bandwidth of LED by CdSe/ZnS quantum dots for visible light communication," *Opt. Exp.*, vol. 24, no. 19, pp. 21577–21586, 2016.
[8] R. Liang *et al.*, "Quantum dots-based flexible films and their application as the phosphor in white light-emitting diodes," *Chem. Mater.*, vol. 26, no. 8, pp. 2595–2600, 2014.
[9] W. Chung, K. Park, H. J. Yu, J. Kim, B. H. Chun, and S. H. Kim, "White emission using mixtures of CdSe quantum dots and PMMA as a phosphor," *Opt. Mater.*, vol. 32, no. 4, pp. 515–521, 2010.
[10] W. Chen *et al.*, "High efficiency and color rendering quantum dots white light emitting diodes optimized by luminescent microspheres incorporating," *J. Nanophoton.*, vol. 5, no. 4, pp. 565–572, 2016.
[11] J. Ryckaert *et al.*, "Selecting the optimal synthesis parameters of InP/CdxZn 1− xSe quantum dots for a hybrid remote phosphor white LED for general lighting applications," *Opt. Exp.*, vol. 25, no. 24, pp. A1009–A1022, 2017.
[12] J. M. Moon, J. S. Kim, B. G. Min, H. M. Kim, and J. S. Yoo, "Optical characteristics and longevity of quantum dot-coated white LED," *Opt. Mater. Exp.*, vol. 4, no. 10, pp. 2174–2181, 2014.

[13] J. Ren, J. Sun, X. Sun, R. Song, Z. Xie, and S. Zhou, "Precisely controlled up/down-conversion liquid and solid state photoluminescence of carbon dots," *Adv. Opt. Mater.*, vol. 6, 2018, Art. no. 1800115.
[14] Y. Wang *et al.*, "High color rendering index trichromatic white and red LEDs prepared from silane-functionalized carbon dots," *J. Mater. Chem. C.*, vol. 5, no. 37, pp. 9629–9637, 2017.
[15] B. Yuan *et al.*, "Highly efficient carbon dots with reversibly switchable green−red emissions for trichromatic white light-emitting diodes," *ASC Appl. Mater. Interfaces*, vol. 10, no. 8, pp. 16005–16014, 2018.
[16] P. Zhang, W. Li, X. Zhai, C. Liu, L. Dai, and W. Liu, "A facile and versatile approach to biocompatible "fluorescent polymers" from polymerizable carbon nanodots," *Chem Commun.*, vol. 48, no. 84, pp. 10431–10433, 2012.
[17] Y. Zheng, Z. Yang, and J. Y. Ying, "Aqueous synthesis of glutathione-capped ZnSe and $Zn_{1-x}Cd_xSe$ alloyed quantum dots," *Adv. Mater.*, vol. 19, no. 11, pp. 1475–1479, 2017.
[18] Y. Wang, X. Li, J. Song, L. Xiao, H. Zeng, and H. Sun, "All-inorganic colloidal perovskite quantum dots: A new class of lasing materials with favorable characteristics," *Adv. Mater.*, vol. 27, no. 44, pp. 7101–7108, 2015.
[19] Y. J. Lee, Y. C. Yao, M. T. Tsai, A. T. Liu, M. D. Yang, and J. T. Lai, "Current matching using CdSe quantum dots to enhance the power conversion efficiency of InGaP/GaAs/Ge tandem solar cells," *Opt. Exp.*, vol. 21, no. S6, pp. A953–A963, 2013.
[20] Y. J. Lee, C. J. Lee, and C. M. Cheng, "Enhancing the conversion efficiency of red emission by spin-coating CdSe quantum dots on the green nanorod light-emitting diode," *Opt. Exp.*, vol. 18, no. S4, pp. A554–A561, 2010.
[21] Y. C. Yao *et al.*, "Coherent and polarized random laser emissions from colloidal CdSe/ZnS quantum dots plasmonically coupled to ellipsoidal Ag nanoparticles," *Adv. Opt. Mater.* vol. 5, 2017, Art. no. 1600746.
[22] H. Xiao, X. Xiao, K. Wang, and K. S. Chiang, "Light-emitting diode conditioned with YAG: Ce^{3+} phosphors and CdSe/ZnS quantum dots for high color-rendering-index white-light generation," in *Proc. Microopt. Conf.*, Tokyo, Japan, 2017, pp. 196–197.
[23] S. Watson *et al.*, "Visible light communications using a directly modulated 422 nm GaN laser diode," *Opt. Lett.*, vol. 38, no. 19, pp. 3792–3794, 2013.
[24] J. J. D. McKendry *et al.*, "Visible-light communications using a CMOS-controlled micro-light-emitting-diode array," *J. Lightw. Technol.*, vol. 30, no. 1, pp. 61–67, 2012.
[25] R. X. Ferreira *et al.*, "High bandwidth GaN-based micro-LEDs for multi-Gb/s visible light communications," *IEEE Photon. Technol. Lett.*, vol. 28, no. 19, pp. 2023–2026, Oct. 2016.
[26] Y. Wang, Y. Wang, N. Chi, J. Yu, and H. Shang, "Demonstration of 575-Mb/s downlink and 225-Mb/s uplink bi-directional SCM-WDM visible light communication using RGB LED and phosphor-based LED," *Opt. Exp.*, vol. 21, no. 1, pp. 1203–1208, 2013.
[27] G. Cossu, A. M. Khalid, P. Choudhury, R. Corsini, and E. Ciaramella, "3.4 Gbit/s visible optical wireless transmission based on RGB LED," *Opt. Exp.*, vol. 20, no. 26, pp. B501–B506, 2012.
[28] Z. T. Li, Y. Tang, Z. Y. Liu, Y. E. Tan, and B. M. Zhu, "Detailed study on pulse-sprayed conformal phosphor configurations for LEDs," *J. Display Technol.*, vol. 9, no. 6, pp. 433–440, 2013.
[29] X. Luo, X. Fu, F. Chen, and H. Zheng, "Phosphor self-heating in phosphor converted light emitting diode packaging," *Int. J. Heat Mass Transfer*, vol. 58, no. 12, pp. 276–281, 2013.
[30] Y. Wang, G. Bu, Y. Wang, T. Zhao, Z. Zhang, and Z. Zhu, "Application of a simulated annealing algorithm to design and optimize a pressure-swing distillation process," *Comput. Chem. Eng.*, vol. 95, pp. 97–107, 2016.
[31] T. Azuma *et al.*, *Method of Measuring and Specifying Colour Rendering Properties of Light Sources*. Paris, France: Commission Int. de L'Eclairage, 1974.
[32] E. F. Schubert, *Light-Emitting Diodes*. New York, NY, USA: Cambridge Univ. Press, 2006.
[33] S. Yi, W. J. Chung, and J. Heo, "Phosphor-in-fluorescent-glasses for high color rendering white light emitting diodes," *J. Amer. Ceram. Soc.*, vol. 100, no. 6, pp. 2378–2381, 2017.
[34] C. H. Yeh, C. W. Chow, H. Y. Chen, J. Chen, and Y. L. Liu, "Adaptive 84.44−190 Mbit/s phosphor-LED wireless communication utilizing no blue filter at practical transmission distance," *Opt. Exp.*, vol. 22, no. 8, pp. 9783–9783, 2014.
[35] C. H. Yeh, Y. L. Liu, and C. W. Chow, "Real-time white-light phosphor-LED visible light communication (VLC) with compact size," *Opt. Exp.*, vol. 21, no. 22, pp. 26192–26197, 2013.
[36] W. Nan *et al.*, "Crystal structure control of zinc-blende CdSe/CdS core/shell nanocrystals: Synthesis and structure-dependent optical properties," *J. Amer. Chem. Soc.*, vol. 134, no. 48, pp. 19685–19693, 2012.
[37] J. Y. Sung, C. W. Chow, and C. H. Yeh, "Is blue optical filter necessary in high speed phosphor-based white light LED visible light communications?" *Opt. Exp.*, vol. 22, no. 17, pp. 20646–20651, 2014.
[38] C. H. Yeh, H. Y. Chen, C. W. Chow, and Y. L. Liu, "Utilization of multi-band OFDM modulation to increase traffic rate of phosphor-LED wireless VLC," *Opt. Exp.*, vol. 23, no. 2, pp. 1133–1138, 2015.
[39] C. W. Hsu, C. W. Chow, I. C. Lu, Y. L. Liu, C. H. Yeh, and Y. Liu, "High speed imaging 3×3 MIMO phosphor white-light LED based visible light communication system," *IEEE Photon. J.*, vol. 8, no. 6, Dec. 2016, Art. no. 7907406.
[40] H. Li, X. Chen, J. Guo, and H. Chen, "A 550 Mbit/s real-time visible light communication system based on phosphorescent white light LED for practical high-speed low-complexity application," *Opt. Exp.*, vol. 22, no. 22, pp. 27203–27213, 2014.
[41] C. W. Chow, Y. Liu, C. H. Yeh, C. Y. Chen, C. N. Lin, and D. Z. Hsu, "Secure communication zone for white-light LED visible light communication," *Opt. Commun.*, vol. 344, pp. 81–85, 2015.
[42] H. Zheng, J. Chen, C. Yu, and M. Gurusamy, "Inverse design of LED arrangement for visible light communication systems," *Opt. Commun.*, vol. 382, pp. 615–623, 2017.
[43] [Online]. Available: https://www.thorlabschina.cn/newgrouppage9.cfm?objectgroup_id =6686